HETEROCYCLES, Vol. 91, No. 4, 2015, pp. 795 - 814. © 2015 The Japan Institute of Heterocyclic Chemistry
Received, 9th February, 2015, Accepted, 9th March, 2015, Published online, 11th March, 2015
DOI: 10.3987/COM-15-13189

SYSTEMATIC INVESTIGATION OF FLUORESCENCE PROPERTIES OF SYMMETRIC AND ASYMMETRIC DIAZOLO[1,2-*a*:2′,1′-*c*]-QUINOXALINE DERIVATIVES

Shoji Matsumoto,* Keisuke Sakamoto, and Motohiro Akazome

Department of Applied Chemistry and Biotechnology, Graduate School of Engineering, Chiba University, 1-33 Yayoicho, Inageku, Chiba 263-8522, Japan; E-mail: smatsumo@faculty.chiba-u.jp

Abstract – The investigation of the synthesis and optical properties of symmetric and asymmetric diazolo[1,2-*a*:2′,1′-*c*]quinoxaline derivatives were systematically examined. The formation of an intramolecular carbon-carbon bond between two azole rings could be achieved by selection of the reaction depending on the type of azole. The absorption and fluorescence spectra revealed the following effects induced by structural changes: 1) introduction of a fused-benzene ring affects the peak shape and the increment of 0-0 transition in the absorption and fluorescence spectra. 2) A hypsochromic shift is induced by substitution of the CH moiety with a nitrogen atom. 3) Introduction of fused-benzene ring(s) is a promising strategy for improving the fluorescence quantum yield of these species. Furthermore, all of the compounds were fluorescent in the solid state, although no systematic trend was found. Investigation of the single crystal structures revealed a diversity of crystal packing arrangements, even in related structures.

INTRODUCTION

The development of organic fluorophores is an important undertaking in many areas of chemistry, biology, and engineering for advancement of functional materials research. A variety of fluorescent materials have been explored, among which planar π-conjugated compounds are particularly attractive for the development of fluorophores.[1] The fluorescence properties of certain planar π-conjugated compounds can be tuned by introducing substituents at the proper positions and by expanding the conjugation. In the modification of the fluorescence of compounds by such methods, the symmetry of the compound is generally maintained based on consideration of the synthesis requirements and/or on simplifying the interpretation of changes in the optical properties. Consequently, there are few detailed and systematic investigations of the differences in the optical properties of symmetric and asymmetric analogs.[2] And it is

important to investigate about the symmetric and asymmetric analogues for revealing the influence on the optical properties, systematically. Our research has focused on unique π-conjugated materials such as dipyrrolo- (**1-nn**) and diindolo[1,2-*a*:2′,1′-*c*]quinoxalines (**1-BB**) (Scheme 1)[3] that have the specific features of rigidity and planarity. Compounds **1-nn** and **1-BB** exhibit good fluorescence quantum yields (Φ_F = 0.34~0.55) with evident differences in the spectral profiles of these two species. Furthermore, we found that replacement of the CH moiety in **1-nn** with a nitrogen atom generated diimidazo[1,2-*a*:2′,1′-*c*]quinoxaline (**2-nn**) that exhibited an increase of the fluorescence quantum yield based on a hypsochromic shift of the fluorescence spectrum compared with **1-nn**,[4] though both species have a C_{2v} symmetric structure. Nevertheless, the remaining symmetric compound, dibenzimidazo[1,2-*a*:2′,1′-*c*]quinoxaline (**2-BB**), has not been synthesized to date. Herein, we report the systematic investigation on the optical properties of the symmetric and asymmetric diazolo[1,2-*a*:2′,1′-*c*]quinoxalines. To evaluate the influence in a systematic manner, desymmetrization is performed herein by two methods: 1) substitution of the CH moiety by a nitrogen atom, and 2) attachment of a fused-benzene ring by developing methods for synthesizing the symmetric and asymmetric compounds (Scheme 1). This study demonstrates that drastic changes of the spectral profile can be obtained by introducing only one benzo-fused ring, and the luminescence can be tuned by changing the number of the replacement by nitrogen atoms. Furthermore, we evaluate the diversity of the solid-state fluorescence and the crystal packing in the structurally related molecules.

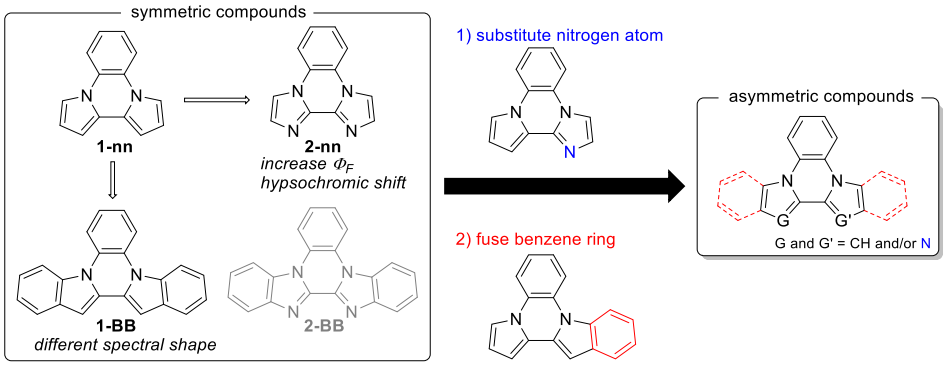

Scheme 1. Groups of symmetric diazolo[1,2-*a*:2′,1′-*c*]quinoxaline derivatives and desymmetrization scheme

RESULT AND DISCUSSION

SYNTHESIS OF DIAZOLO[1,2-*a*:2′,1′-*c*]QUINOXALINES

The synthetic strategies employed herein offer the merits of being simple and straightforward, involving introduction of two heteroaromatic rings into the benzene ring at the *ortho* position and coupling with these rings. To obtain the asymmetric structures, different aromatic rings were introduced at the ortho position. Fortunately, the synthesis of 1-(*o*-bromophenyl)pyrrole and 1-(*o*-bromophenyl)benzimidazole in

excellent yields was reported by Lautens[5] and Glorius,[6] respectively. The copper-catalyzed coupling reaction was efficient for generating the precursors of symmetric **1-nn** and **2-nn**. Therefore, the coupling reactions of 1-(*o*-bromophenyl)pyrrole and 1-(*o*-bromophenyl)benzimidazole with various nitrogen-containing heteroaromatics were conducted by copper(I) catalysis. Initial screening of the various reaction conditions such as the catalyst, ligand, base, solvent, and reaction temperature led to successful synthesis of the asymmetric *ortho*-substituted benzenes (Scheme 2).

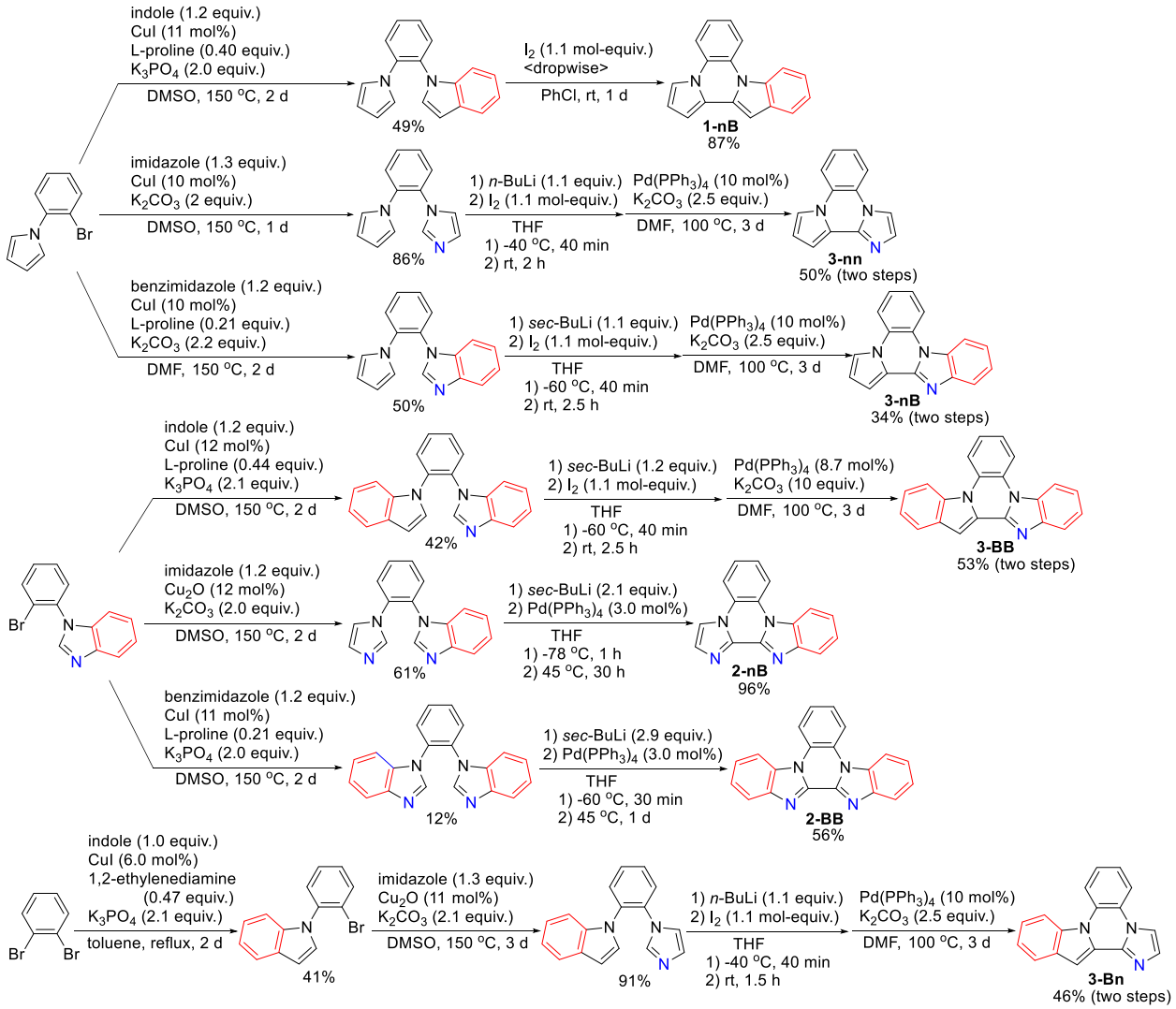

Scheme 2. Formation of various quinoxaline derivatives

In a previous investigation,[3,4] we successfully executed the coupling reactions between two heteroaromatics by the iodine oxidation (for pyrrole-pyrrole and indole-indole connections depicted as **1**), and by the formation of a dianion followed by Pd catalysis (for imidazole-imidazole connection depicted as **2**). By utilizing the same reaction protocols, the corresponding asymmetric compounds (**1-nB**, **2-nB**, and **2-BB**) were also obtained. This implies that the coupling reaction is not affected by the presence of the fused-benzene ring. To make the pyrrole-imidazole type compounds (**3**) by the coupling reaction, the

conditions that successfully generated **1** and **2** were examined; however, the desired reaction did not occur. Therefore, **3** was synthesized by iodination at the imidazole moiety followed by coupling with $Pd(PPh_3)_4$ in the presence of K_2CO_3. This protocol could also be applied to synthesis of **3** with or without fused benzenes.

To achieve the systematic investigation, we tried to synthesize **3-Bn**. *o*-Dibromobenzene was first reacted with 1 equiv. of indole in the presence of CuI catalyst[7] to generate *o*-bromo substituted 1- phenylindole in 41% yield. Further imidazole coupling reactions and C-C bond formation between the indole and imidazole were achieved to give **3-Bn** by the method mentioned above.

ABSORPTION AND FLUORESCENCE OF DIAZOLO[1,2-*a*:2′,1′-*c*]QUINOXALINES IN SOLUTION

The absorption and fluorescence spectra of all compounds were measured in THF (Table 1 and Figure 1). Comparison of the optical properties of the compounds without fused-benzene rings (**1-nn**, **3-nn**, and **2-nn**) (Figure 1a) demonstrated diffuse absorption peaks around 310 nm and broadened fluorescence peaks. Introduction of the nitrogen atoms induced hypsochromic shifts of the maximum absorption (λ_{max}) and fluorescence (λ_{em}) peaks (entries 1, 2, and 3). The impact of substituting one CH group with a nitrogen atom on λ_{max} and λ_{em} was more profound than that of the subsequent substitution. The differences in the peak positions, $\Delta\lambda_{max}$ (8 nm) and $\Delta\lambda_{em}$ (28 nm), of **1-nn** versus **3-nn** were more pronounced than those of **3-nn** versus **2-nn** ($\Delta\lambda_{max}$ = 4 nm and $\Delta\lambda_{em}$ = 21 nm). A higher quantum yield (Φ_F) was obtained with the symmetric structure, whereas asymmetric **3-nn** gave rise to a low Φ_F (entry 2). The Φ_F of **2-nn** was excellent (0.72).

The compounds bearing one fused-benzene ring (**1-nB**, **3-Bn**, **3-nB**, and **2-nB**) absorbed at longer wavelengths (Figure 1b). Introduction of the fused-benzene ring effectively extends the π-conjugated system. But **1-nB**, **3-Bn**, and **3-nB** emitted at shorter wavelengths than the **1-nn**, **3-nn**, and **2-nn** congeners. Notably, fine structures were observed in the absorption as well as fluorescence spectra, which is a marked difference relative to the non-fused compounds. Considering the large overlap of the edges of the absorption and fluorescence peaks, emission from the 0-0 band should be efficient. As the results, smaller Stokes shifts of **1-nB**, **3-Bn**, **3-nB**, and **2-nB** (578, 223, 580, and 338 cm^{-1}, respectively) were obtained than those of **1-nn**, **3-nn**, and **2-nn** (7114, 6176, and 5115 cm^{-1}, respectively). It is suggested that the introduction to the fused benzene-ring would decrease in the structural change between the ground and excited states. In the case of **1-nB** and **3-Bn** in which the fused-benzene ring is present on the pyrrole moiety, λ_{max} and λ_{em} were observed around 365 nm and 370 nm, respectively (entries 4 and 5), whereas the maximum absorption and emission occurred at shorter wavelengths in the case of **3-nB** and **2-nB** bearing the fused-benzene ring on the imidazole moiety (λ_{max} ~ 340 nm and λ_{em} ~ 350 nm) (entries

6 and 7). Furthermore, substitution of the nitrogen atom on the pyrrole ring produced a small shift of λ_{max} and λ_{em} relative to the non-fused compounds (vide supra) ($\Delta\lambda_{max}$ = 3 nm and $\Delta\lambda_{em}$ = 8 nm for **1-nB** vs. **3-Bn**, and $\Delta\lambda_{max}$ = 2 nm and $\Delta\lambda_{em}$ = 5 nm for **3-nB** vs. **2-nB**). These results suggest that the position of the fused-benzene ring strongly affects the absorption and fluorescence peaks. The singly fused compounds all have asymmetric structures and exhibited medium Φ_F values (~0.50), except for **1-nB** (Φ_F = 0.32). Thus, introduction of the fused benzene ring positively affected Φ_F, which will lead to the small structural change between the ground and excited states.

Fine structures were also observed in the absorption and fluorescence spectra of the doubly fused compounds (**1-BB**, **3-BB**, and **2-BB**) (Figure 1c). The absorption and fluorescence spectra of **1-BB** and **3-BB** containing the indole moiety were largely similar (entries 8 and 9). Furthermore, comparison of **1-BB**, **3-BB**, **1-nB**, and **3-Bn** shows small changes in the peaks ($\Delta\lambda$ = 2~5 nm) due to introduction of the additional fused-benzene ring. Thus, the absorption and fluorescence spectra were influenced by the presence of the indole moiety in the series of diazolo[1,2-*a*:2′,1′-*c*]quinoxalines. In contrast, a bathochromic shift was observed in the case of the compounds bearing the benzimidazole moiety (entry 6 vs. 9, and entry 7 vs. 10). Medium values of Φ_F were obtained for **1-BB**, **3-BB**, and **2-BB**; these values are slightly smaller than those of the singly fused compounds, except for **1-nB**.

Table 1. Optical properties of evaluated compounds

Entry	Compound	λ_{max} (nm)[a] [ε_{max} (M^{-1} cm^{-1})]	λ_{em} (nm)[b] [Φ_F][c]	λ_{em} in the solid state (nm)[d] [Φ_F][e]
1	**1-nn**	321 [10,600][f]	416 [0.43][f]	417 [0.02]
2	**3-nn**	313 [8,900]	388 [0.37]	376(sh), 404, 426, 453(sh) [0.12]
3	**2-nn**	309 [9,400][g]	367 [0.72][g]	380, 397, 421(sh) [0.36]
4	**1-nB**	368 [13,000]	376, 396[h] [0.32]	441 [0.03]
5	**3-Bn**	365 [13,700]	368, 389, 411[h] [0.52]	455 [0.05]
6	**3-nB**	344 [17,200]	351,367, 384(sh)[h] [0.52]	383(sh), 437, 500 [0.06]
7	**2-nB**	342 [15,600]	346, 362, 381[h] [0.55]	379, 399, 419, 466(sh) [0.04]
8	**1-BB**	372 [46,000][f]	372, 396, 420[h] [0.55][f]	421(sh), 466, 498(sh) [0.05]
9	**3-BB**	370 [25,400]	372, 394, 418[h] [0.49]	415, 435, 464(sh) [0.10]
10	**2-BB**	354 [33,600]	356, 375, 396[h] [0.42]	454 [0.02]

[a] Measured in THF (3.0×10^{-5} M). [b] Measured in THF (3.0×10^{-5} M) excited at λ_{max}. [c] Determined using *p*-terphenyl (Φ_F = 0.87, excited at 265 nm) as a standard. [d] Spectra acquired with 311 nm excitation were measured using the sample sandwiched by quartz glass and black plastic plate. [e] Determined using the sample sandwiched by KBr plates with a calibrated integration sphere system. [f] Ref. 3. [g] Ref. 4. [h] Excited at 265 nm to observe 0-0 transition.

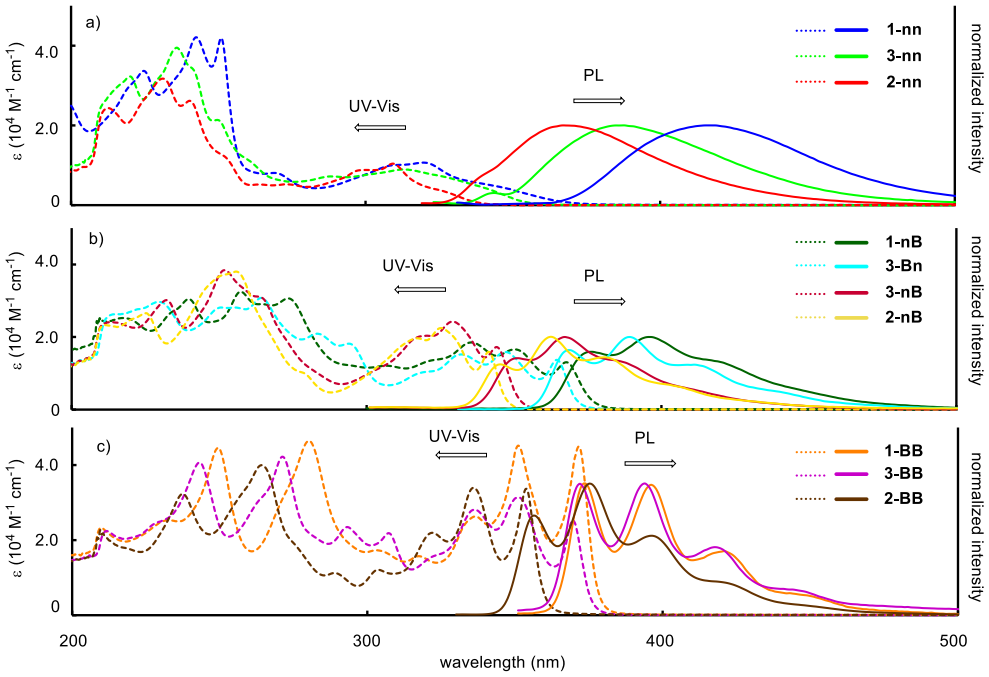

Figure 1. Absorption (3.0×10^{-5} M in THF; dashed lines) and fluorescence (3.0×10^{-7} M in THF; plane lines) spectra of a) non-fused compounds (**1-nn**, **2-nn**, **3-nn**), b) singly fused compounds (**1-nB**, **3-Bn**, **3-nB**, **2-nB**), and doubly fused compounds (**1-BB**, **3-BB**, **2-BB**)

The molecular orbitals were simulated based on density functional theory (DFT) and time-dependent DFT (TDDFT) calculations at the B3LYP/6-31+G level using the Gaussian® 09 program.[8] The orbitals obtained using the DFT and TDDFT calculations were similar in terms of the HOMO and LUMO for all molecules, except for the HOMO of **2-BB**[9] (Figure 2 and Figure S1 in Supporting Information), which implies that the structural change between in the ground and excited state is little affected on their orbitals. The HOMO of the pyrrole and imidazole moieties had a nodal plane between the 3 and 4 positions, and between the 1 and 5 positions. The double bond character between the phenylene and pyrrole or imidazole groups arises mainly in the LUMO state because the orbitals are present on the bond connecting the two rings. The orbitals of the benzene-fused compounds differed based on the structures. The HOMOs were primarily localized on the biazole moiety, whereas the LUMOs were spread over the entire molecule. The HOMO and LUMO were localized on the fused benzene, which may enhance the transition between the HOMO and LUMO, leading to the large absorption coefficient (ε_{max}) and Φ_F. However, the actual value of Φ_F would be determined by the balance between the probability of the transition and thermal vibration of the molecules because decay from the excited state includes radiative as well as non-radiative decay. The both energy of HOMO and LUMO of the compounds with (benz)imidazole moieties gave lower value than that of the analogue with pyrrole and indole moieties. But the decrease of LUMO energy were more efficient than that of HOMO energy. Thus, the bathochromic sift of the compounds bearing additional nitrogen atom would be obtained.

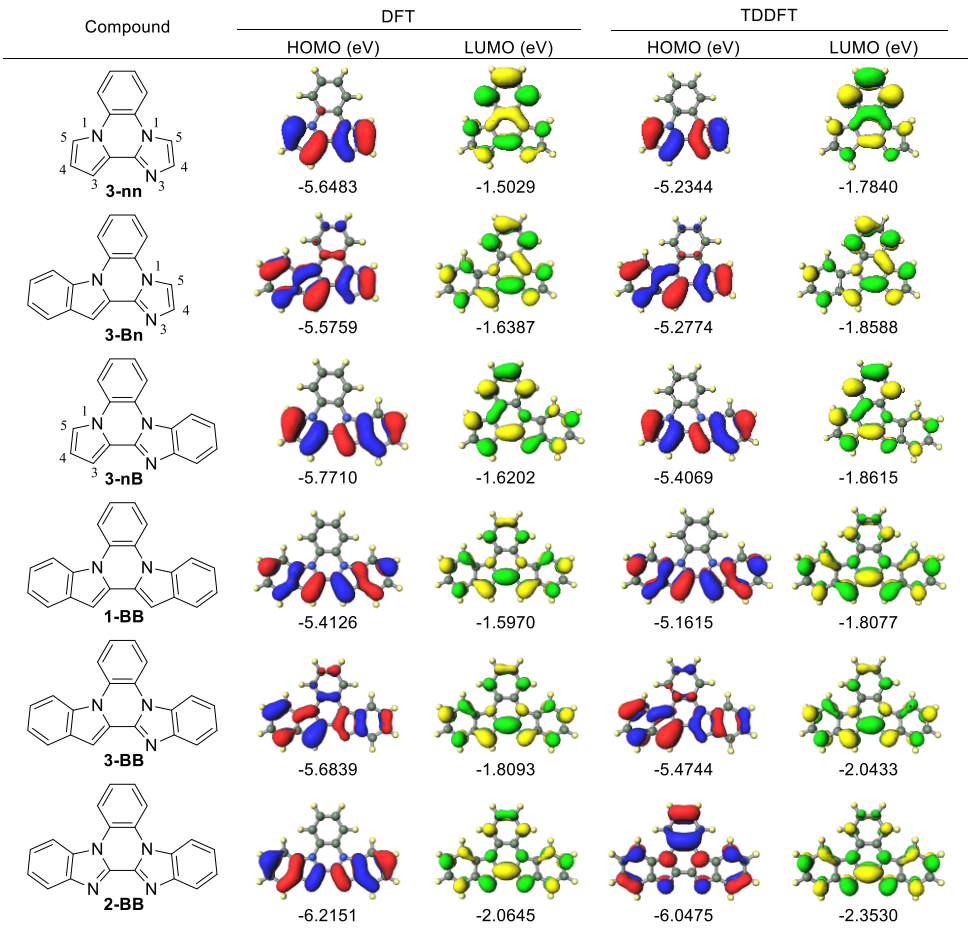

Figure 2. The HOMO, LUMO, and their energies of **3-nn**, **3-Bn**, **3-nB**, **1-BB**, **3-BB**, and **2-BB** estimated by DFT and TDDFT (nstate =10) calculation after structural optimization at the B3LYP/6-31+G level

Based on these results, the following deductions concerning the optical properties of the symmetric and asymmetric diazolo[1,2-*a*:2′,1′-*c*]quinoxalines in solution could be made: 1) the fused-benzene ring has a strong impact on the absorption and fluorescence spectra in terms of the peak shapes and energy. 2) A hypsochromic shift is induced by substituting the CH moiety with a nitrogen atom. 3) Introduction of fused-benzene ring(s) is a promising strategy for improving the fluorescence quantum yield.

FLUORESCENCE CHARACTER IN THE SOLID STATE AND SINGLE CRYSTAL X-RAY STRUCTURE OF DIAZOLO[1,2-*a*:2′,1′-*c*]QUINOXALINES

A number of aromatic compounds having good planarity are not fluorescent in the solid state because of fluorescence quenching due to intermolecular interactions such as excimer formation derived from π–π interaction.[10,11] The compounds discussed in this paper have good planarity but exhibit medium to good fluorescence quantum yields in solution. Therefore, the fluorescence properties of these species in the solid state were examined. The results are summarized in Table 1 and Figure 3. All of the compounds were fluorescent in the solid state although the quantum yields were generally low. The maximum

quantum yield (0.36) was obtained with **2-nn**. Unlike the case in solution, there was no systematic trend in the peak shapes and energies. This would be attributed to variations in the interactions in the solid state.

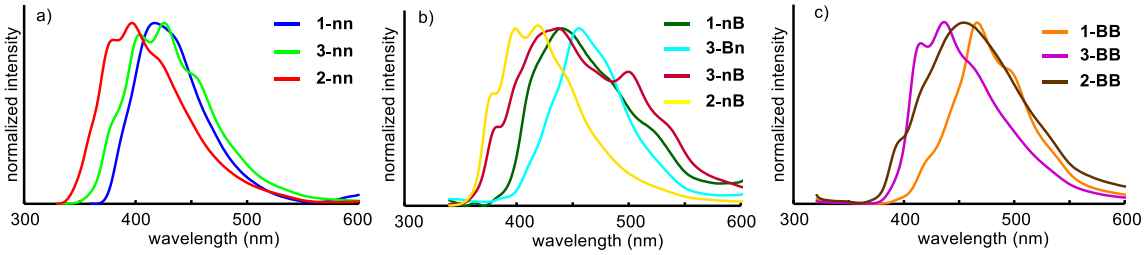

Figure 3. Fluorescence spectra of a) non-fused compounds (**1-nn**, **2-nn**, **3-nn**), b) singly fused compounds (**1-nB**, **3-Bn**, **3-nB**, **2-nB**), and doubly fused compounds (**1-BB**, **3-BB**, **2-BB**) in the solid state

Fortunately, crystals of **1-nn** and **3-nn** suitable for single crystal X-ray analysis were obtained. **1-nn** gave rise to two types of molecular structures (**1-nn** (I) and **1-nn** (II)), whereas **3-nn** adopted a single molecular structure in the symmetric unit of the crystal structure (Figure 4). The length of the C-N bond formed by exchange of the CH group in the pyrrole ring with a nitrogen atom (1.32 Å) was slightly shortened relative to those of the pyrrole moiety (1.38~1.36 Å). The angles between the biazole plane and phenylene plane were within 2° (1.3° for **1-nn** (I), 1.8° for **1-nn** (II), **1-nn** (I), 1.8° for **1-nn** (II), and 1.9° for **3-nn**), and the torsional angles of the two azoles were also observed to be 1.6°, 0.5°, and 0.8° for **1-nn** (I), **1-nn** (II), and **3-nn**, respectively. Thus, the hydrogen atom attached to **1-nn** has no influence on the molecular planarity, and both molecules showed good planarity.

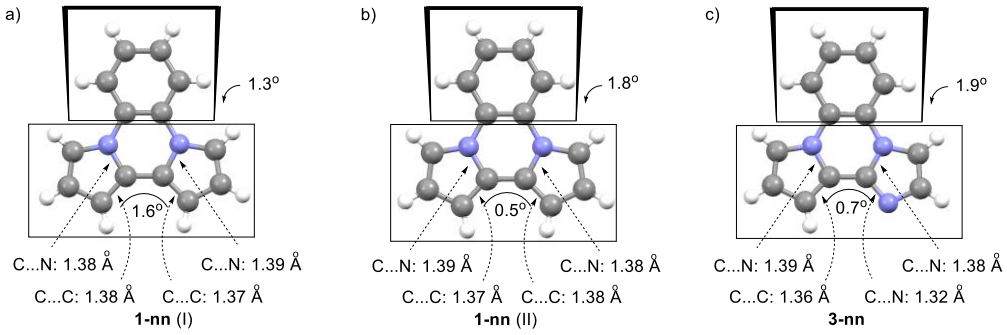

Figure 4. Molecular structure of a) **1-nn** (I), b) **1-nn** (II), and c) **3-nn** obtained by single crystal X-ray crystallographic analysis

Despite the similarity of the structures, the packing structure was significantly different for **1-nn** and **3-nn**. In the case of **1-nn**, two structurally different molecules are aligned in two π planes with a tilt of 86.9° (Figure 5a). The molecules interact via several edge-to-face alignments held by hydrogen and π plane interaction in the benzene as well as pyrrole moieties. The molecules formed a layer structure (Figure 5c).

In each layer, the orientation of the molecules was the same; one pyrrole ring was situated close to the position between the benzene and pyrrole rings of another molecule. However, there was small overlap of the π plane in the layers (Figures 5d and 5e). Based on these results, less interaction between the molecules resulted in greater similarity of λ_{em} in solution and in the solid state.

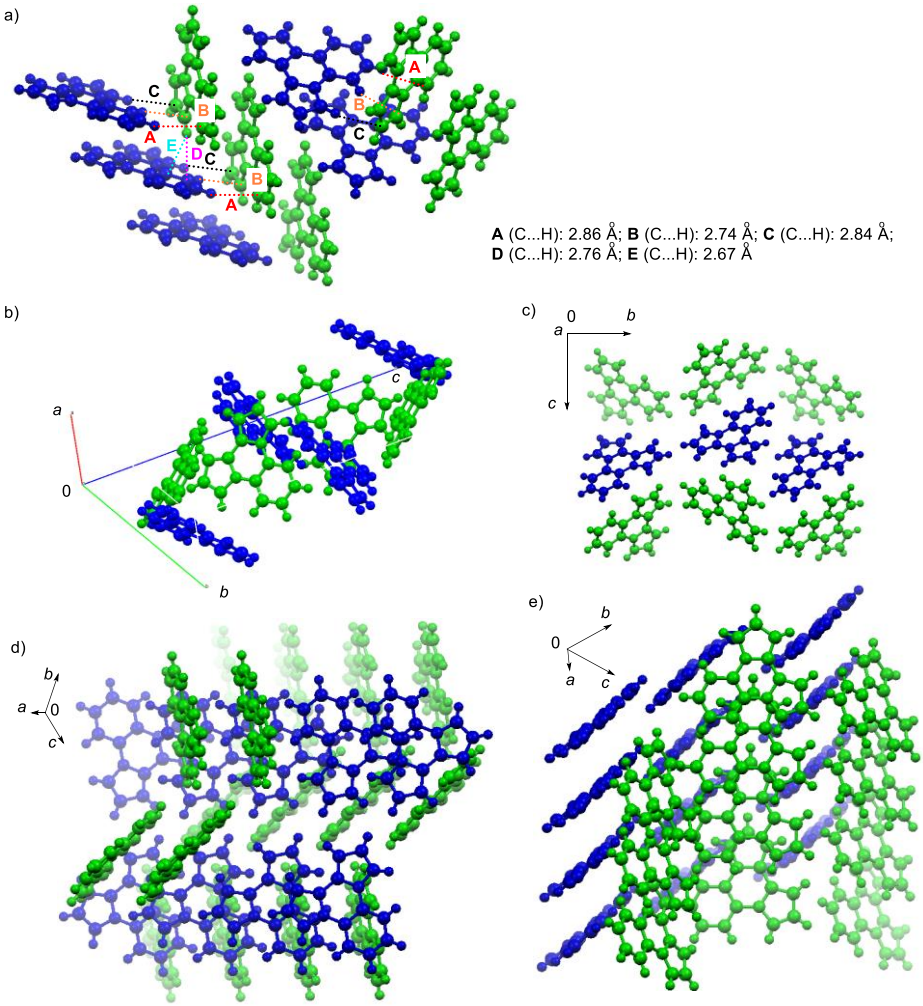

Figure 5. Single crystal X-ray structure of **1-nn**. The molecules of **1-nn** (I) and **1-nn** (II) in Figure 3 are shown in green and blue, respectively. a) Interaction between two molecules, b) unit cell, c) the layer structures, and top view of the layer structures of d) molecule represented in blue (**1-nn** (II)) and of e) molecule represented in green (**1-nn** (I))

In sharp contrast to **1-nn**, π-π stacking was observed in the crystal structure of **3-nn** (Figures 6a and 6c). Two types of stacking modes were observed (type A and type B). Each stack of molecules was oriented with C_2 symmetry (Figure 6a). The quinoxaline rings overlapped with a slight shift of the alignment in both stacking modes. The center of each molecule was also shifted toward the stacking axis in the case of type A stacking, whereas complete overlap of the centers was observed in type B stacking. The distance between the two molecules was different. In type A stacking, π-π interactions were plausibly operative between molecules because the distance between the carbon atoms (distances shown in **A**, **B**, and **C** in

Figure 6c) was within the sum of the van der Waals radii of sp^2 carbon atoms where the radius is 1.77 Å[12] and the distance between each π plane was estimated to be 3.32 Å as the average of the distance between carbon or nitrogen atoms and another π plane. Therefore, attractive π-π stacking was observed. In type B stacking, the distance between molecules was somewhat longer, and certain of the distances between carbon atoms (distance shown in **B'** and **C'** in Figure 6c) exceeded the sum of the van der Waals radii. However, the distance between π planes (3.41 Å) was within the sum of the van der Waals radii (3.54 Å). Thus, type B stacking was stabilized by π-π interactions. In support of this proposal, calculations for the type A and type B models predicted the presence of the HOMO and LUMO on both molecules in the different orbital structures versus the orbitals of the single molecule (Figure S3).

Therefore, it was concluded that **3-nn** was stabilized by π-π stacking in an *h*-aggregated manner. Some studies reported fluorescence from *h*-aggregated compounds,[13,14] and a bathochromic shift was also observed. In the case of **3-nn**, the maximum fluorescence in the solid state (426 nm) was actually bathochromically shifted relative to that in solution (388 nm). Furthermore, the fine structure observed in the solid state would exclude fluorescence from the excimer in the solid state.

Focusing on the side molecules, the hydrogens of the azole moieties in type A are positioned near the nitrogen atom of the imidazole of the side molecule. The distance between the nitrogen and hydrogen (distance shown in **D** and **E** in Figure 6d) is close to the sum of the van der Waals radii of nitrogen and hydrogen (1.55 Å (1.63 Å in tetrazole) and 1.00 Å, respectively),[12] although the orientation is not consistent with hydrogen-bonding interaction using the lone pair on the nitrogen atom. Additionally, the hydrogens are located at the α position of the nitrogen atom of the azole rings; this positioning should increase the acidity. Therefore, there might be static interaction between the hydrogens and nitrogen in neighboring molecules. The difference in the crystal structure of **1-nn** and **3-nn** is thought to be derived from these different interactions. We could not find any reason for the difference of Φ_F between **1-nn** and **3-nn** in the solid state. But various interactions in **3-nn** would lead to low vibrational quenching to give higer Φ_F.

CONCLUSION

In conclusion, symmetric and asymmetric diazolo[1,2-*a*:2′,1′-*c*]quinoxaline derivatives were systematically synthesized; carbon-carbon bond formation between two azoles was achieved by the method suited to the type of azole. The reaction between two pyrroles was utilized in the oxidative reaction with iodine. In the case of two imidazoles, formation of the dianion followed by the coupling reaction employing the palladium catalyst was preferable. Furthermore, the reaction between pyrrole and imidazole was amenable to iodination at the imidazole moiety, followed by the coupling reaction. The optical properties of the resulting quinoxalines were also systematically evaluated. It was found that

introduction of a fused benzene, especially on pyrrole moiety, and substitution of a nitrogen atom into the structure had a strong impact on the absorption and fluorescence in solution. Although no trend could be defined for the fluorescence characteristics in the solid state, the diversity of the fluorescence spectra and the crystalline structure of these species was demonstrated. These findings may potentially be utilized as guidelines in the design of new fluorophores.

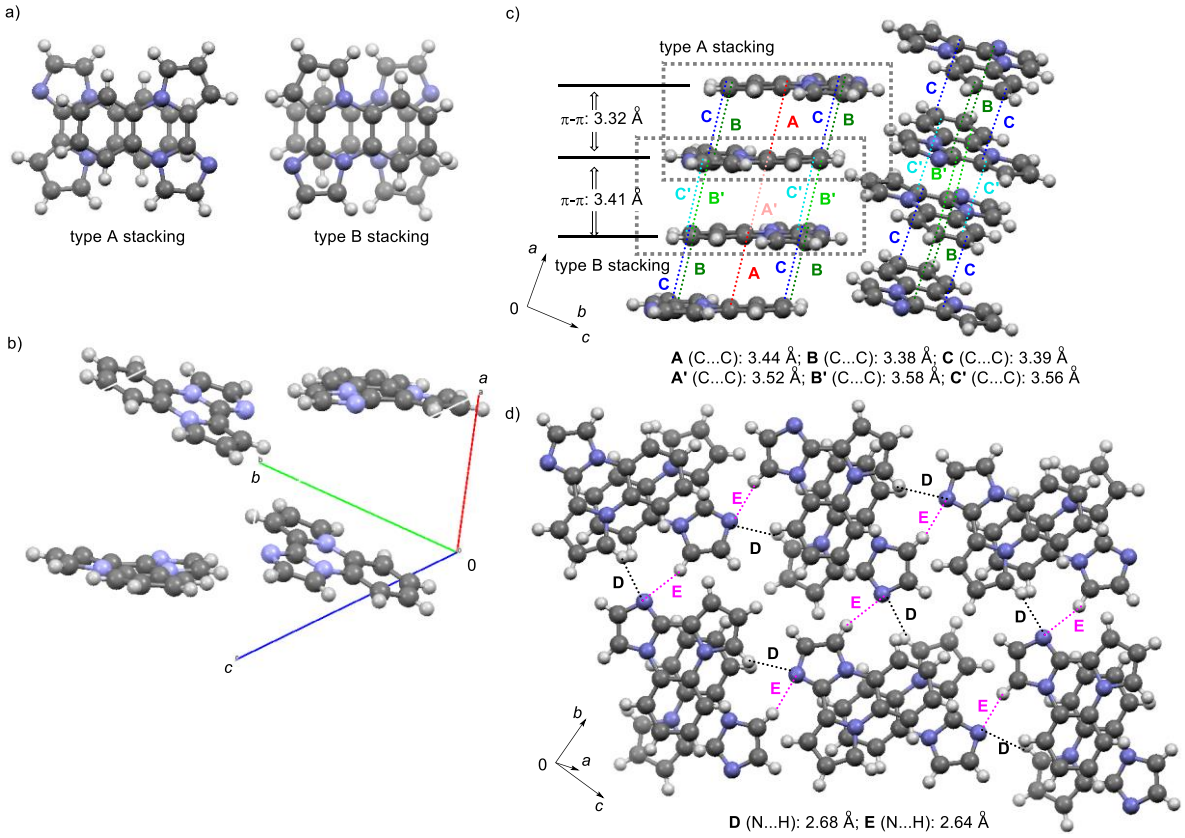

Figure 6. Single crystal X-ray structure of **3-nn**. a) The π-π stacking modes (type A and B), b) unit cell, c) packing structure and carbon-carbon and π plane distances in both stacking modes, and d) short contact between neighboring molecules

EXPERIMENTAL

General: Melting points were determined with Yanaco MP-J3 and values were uncorrected. ^{1}H and ^{13}C NMR measurements were performed on a Varian GEMINI 2000 (300 MHz) spectrometer. Chemical shifts (δ) of ^{1}H NMR were expressed in parts per million downfield from tetramethylsilane in $CDCl_3$ (δ = 0) or DMSO-d_5 (δ = 2.49) as an internal standard. Multiplicities are indicated as s (singlet), d (doublet), t (triplet), q (quartet), m (multiplet), and coupling constants (*J*) are reported in hertz units. Chemical shifts (δ) of ^{13}C NMR are expressed in parts per million downfield or upfield from $CDCl_3$ (δ = 77.0) or DMSO-d_6 (δ = 39.6) as an internal standard. Infrared spectra (IR) spectra were recorded on a JASCO FT/IR-460 plus spectrometer in KBr disk. Mass spectra were carried out on a THERMO Scientific

Exactive in Center for Analytical Instrumentation, Chiba University. Absorption spectra were measured with quartz cell (1 cm × 1 cm) on a JASCO V570 spectrophotometer. Fluorescence spectra in solution were measured with quartz cell (1 cm × 1 cm) on a JASCO FP-6600 spectrofluorometer. Absolute fluorescence quantum yield in the solid state was measured on a JASCO IFL-533 integrating sphere unit. Analytical thin-layer chromatography (TLC) was performed on glass plates that had been pre-coated with silica gel (0.25 mm layer thickness). Column chromatography was performed on 70–230 mesh silica gel. Preparative GPC was performed on JAIGEL-1H and 2H with a LC-908 (Japan Analytical Industry, Co. Ltd.). Anhydrous toluene was distilled from sodium hydride and was stored with MS 4 Å. Anhydrous THF was distilled from sodium benzophenone ketyl immediately prior to use. Anhydrous DMF was distilled from P_2O_5 under reduced pressure and was stored with MS 4 Å. Other chemical materials were used directly as obtained commercially.

Synthesis of 1-(2-(1*H*-Pyrrol-1-yl)phenyl)-1*H*-indole:[15] To a solution of 1-(2-bromophenyl)-1*H*-pyrrole[5] (3.963 g, 17.9 mmol), 1*H*-indole (2.524 g, 21.5 mmol), CuI (0.355 g, 1.86 mmol), K_3PO_4 (7.579 g, 35.7 mmol), and L-proline (0.826 g, 7.17 mmol) in DMSO (40 mL) was heated at 150 °C for 2 d. After cooling down to room temperature, to the reaction mixture was added EtOAc (30 mL) and brine (30 mL). After being extracted with EtOAc (30 mL × 4), the organic layer was washed with brine (30 mL × 3). After drying with $MgSO_4$ and evaporation, the residue was subject to column chromatography on SiO_2 (hexane : $CHCl_3$ = 5 : 1) to give 1-(2-(1*H*-pyrrol-1-yl)phenyl)-1*H*-indole (2.285 g, 8.85 mmol, 49%) as pale brown solid. Recrystallization from hexane and $CHCl_3$ gave colorless plate crystals: mp 129–130 °C; ^{1}H NMR (300 MHz, $CDCl_3$) δ 6.06 (t, *J* = 2.1 Hz, 2H), 6.41 (t, *J* = 2.1 Hz, 2H), 6.54 (d, *J* = 3.2 Hz, 1H), 6.77 (d, *J* = 3.3 Hz, 1H), 7.10-7.23 (m, 3H), 7.37-7.54 (m, 4H), 7.61 (m, 1H); ^{13}C NMR (75 MHz, $CDCl_3$) δ 103.9, 109.8, 110.0, 120.3, 120.4, 120.7, 120.86, 120.95, 122.3, 126.4, 127.2, 127.8, 128.4, 128.6, 128.6, 132.9, 136.5, 137.1; IR (KBr) 3103, 1956, 1925, 1896, 1815, 1785, 1722, 1600, 1585, 1515, 1461, 1393, 1354, 1331, 1319, 1246, 1231, 1212, 1137, 1102, 1068, 1016, 958, 948, 921, 853, 840, 774, 740, 627, 613 cm^{-1}. HRMS (ESI) Calcd for $C_{18}H_{15}N_2$: $[M+H]^+$. 259.1230, found: *m*/*z* 259.1227.

Synthesis of 1-(2-(1*H*-Pyrrol-1-yl)phenyl)-1*H*-imidazole:[16] To a solution of 1-(2-bromophenyl)-1*H*-pyrrole (4.435 g, 20.1 mmol), 1*H*-imidazole (1.785 g, 26.2 mmol), Cu_2O (0.291 g, 2.04 mmol), and K_2CO_3 (5.538 g, 40.0 mmol) in DMSO (40 mL) was heated at 150 °C for 2 d. After cooling down to room temperature, to the reaction mixture was added EtOAc (30 mL) and brine (30 mL). After being extracted with EtOAc (30 mL × 4), the organic layer was washed with brine (30 mL × 3). After drying with $MgSO_4$ and evaporation, the residue was subject to column chromatography on SiO_2 (hexane : EtOAc = 2 : 1 to only EtOAc) to give 1-(2-(1*H*-pyrrol-1-yl)phenyl)-1*H*-imidazole (3.606 g, 17.2 mmol, 86%) as yellow solid. Recrystallization from hexane and $CHCl_3$ gave pale brown cubic crystals: mp 81–

82 °C; ^{1}H NMR (300 MHz, $CDCl_3$) δ 6.23 (t, *J* = 2.0 Hz, 2H), 6.52 (t, *J* = 2.0 Hz, 2H), 6.76 (s, 1H), 7.07 (s, 1H), 7.34 (s, 1H), 7.40-7.47 (m, 4H); ^{13}C NMR (75 MHz, $CDCl_3$) δ 110.5, 119.2, 120.9, 126.3, 127.1, 128.0, 128.9, 129.9, 132.0, 135.4, 136.6; IR (KBr) 3130, 3106, 3091, 1602, 1586, 1513, 1487, 1333, 1314, 1248, 1236, 1117, 1076, 1069, 1057, 1078, 923, 903, 826, 814, 780, 749, 851, 662, 638 cm^{-1}. HRMS (ESI) Calcd for $C_{13}H_{12}N_2$: $[M+H]^+$. 210.1026; found: *m*/*z* 210.1022.

Synthesis of 1-(2-(1*H*-Pyrrol-1-yl)phenyl)-1*H*-benzo[*d*]imidazole:[16] To a solution of 1-(2-bromophenyl)-1*H*-pyrrole (1.120 g, 5.04 mmol), 1*H*-benzo[*d*]imidazole (0.714 g, 6.04 mmol), CuI (99.0 mg, 0.520 mmol), K_2CO_3 (1.392 g, 10.1 mmol), and L-proline (0.119 g, 1.04 mmol) in DMSO (5 mL) was heated at 150 °C for 3 d. After cooling down to room temperature, to the reaction mixture was added EtOAc (5 mL) and brine (10 mL). After being extracted with EtOAc (10 mL × 4), the organic layer was washed with brine (10 mL). After drying with $MgSO_4$ and evaporation, the residue was subject to column chromatography on SiO_2 (hexane : EtOAc = 4 : 1 to 1.5 : 1) to give 1-(2-(1*H*-pyrrol-1-yl)phenyl)-1*H*-benzo[*d*]imidazole (0.659 g, 2.54 mmol, 50%) as brown solid. Recrystallization from hexane and $CHCl_3$ gave pale red cubic crystals: mp 146–148 °C; ^{1}H NMR (300 MHz, $CDCl_3$) δ 6.09 (t, *J* = 2.1 Hz, 2H), 6.43 (t, *J* = 2.2 Hz, 2H), 7.25-7.31 (m, 3H), 7.47-7.56 (m, 5H), 7.81 (d, *J* = 7.5 Hz, 1H); ^{13}C NMR (75 MHz, $CDCl_3$) δ 109.7, 110.6, 120.3, 120.6, 122.7, 123.7, 126.9, 127.70, 127.75, 129.5, 130.0, 133.9, 136.8, 142.1, 143.2; IR (KBr): 3100, 3089, 3062, 1744, 1611, 1600, 1514, 1485, 1468, 1458, 1333, 1318, 1312, 1285, 1229, 1200, 1145, 1101, 1070, 1018, 924, 877, 785, 762, 735, 722, 634, 629, 617 cm^{-1}. HRMS (ESI) Calcd for $C_{17}H_{14}N_3$: $[M+H]^+$. 260.1182, found: *m*/*z* 260.1179.

Synthesis of 1-(2-(1*H*-Indol-1-yl)phenyl)-1*H*-benzo[*d*]imidazole:[16] To a solution of 1-(2-bromophenyl)-1*H*-benzo[*d*]imidazole[6] (2.077 g, 7.60 mmol), 1*H*-indole (1.100 g, 9.39 mmol), CuI (0.174 g, 0.911 mmol), K_3PO_4 (3.424 g, 16.1 mmol), and L-proline (0.387 g, 3.36 mmol) in DMSO (50 mL) was heated at 150 °C for 2 d. After cooling down to room temperature, to the reaction mixture was added EtOAc (5 mL) and brine (10 mL). After being extracted with EtOAc (10 mL × 4), the organic layer was washed with brine (10 mL). After drying with $MgSO_4$ and evaporation, the residue was subject to column chromatography on SiO_2 (hexane : EtOAc = 3 : 1 to 1 : 1) to give 1-(2-(1*H*-indol-1-yl)phenyl)-1*H*-benzo[*d*]imidazole (0.982 g, 3.17 mmol, 42%) as red solid. Recrystallization from hexane and EtOAc gave pale red plate crystals: mp 162–163 °C; ^{1}H NMR (300 MHz, $CDCl_3$) δ 6.39 (d, *J* = 3.2 Hz, 1H), 6.60 (d, *J* = 3.3 Hz, 1H), 7.07-7.10 (m, 2H), 7.17-7.28 (m, 4H), 7.34 (s, 1H), 7.51-7.63 (m, 4H), 7.71 (t, *J* = 7.1 Hz, 2H); ^{13}C NMR (75 MHz, $CDCl_3$) δ 104.7, 109.4, 109.7, 120.4, 120.6, 121.2, 122.66, 122.68, 123.7, 127.1, 127.7, 128.56, 128.63, 128.9, 129.3, 131.9, 133.7, 134.8, 136.3, 142.1, 143.2; IR (KBr) 3124, 3048, 1609, 1594, 1517, 1507, 1483, 1465, 1454, 1330, 1304, 1287, 1240, 1221, 1213, 1136, 1003, 980, 887, 854, 789, 779, 764, 743, 720 cm^{-1}. HRMS (ESI) Calcd for $C_{21}H_{16}N_3$: $[M+H]^+$. 310.1339, found: *m*/*z* 310.1332.

Synthesis of 1-(2-(1*H*-Imidazol-1-yl)phenyl)-1*H*-benzo[*d*]imidazole:[17] To a solution of 1-(2-bromophenyl)-1*H*-benzo[*d*]imidazole (4.761 g, 17.5 mmol), 1*H*-imidazole (1.445 g, 21.2 mmol), Cu_2O (0.306 g, 2.14 mmol), and K_2CO_3 (4.877 g, 35.3 mmol) in DMSO (50 mL) was heated at 150 °C for 2 d. After cooling down to room temperature, to the reaction mixture was added EtOAc (50 mL), brine (50 mL), and 1,2-ethylenedamine (30 mL). After being extracted with EtOAc (50 mL × 4) and $CHCl_3$ (50 mL × 3), the organic layer was washed with brine (50 mL × 2). After drying with $MgSO_4$ and evaporation, the residue was subject to column chromatography on SiO_2 (only EtOAc) to give 1-(2-(1*H*-imidazol-1-yl)phenyl)-1*H*-benzo[*d*]imidazole (2.776 g, 10.7 mmol, 61%) as yellow solid. Recrystallization from hexane and EtOAc gave pale brown cubic crystals: mp 131–132 °C; ^{1}H NMR (300 MHz, $CDCl_3$) δ 6.60 (s, 1H), 6.92 (s, 1H), 7.15 (d, *J* = 7.7 Hz, 1H), 7.25 (t, *J* = 7.0 Hz, 1H), 7.30 (t, *J* = 7.1 Hz, 1H), 7.41 (s, 1H), 7.57-7.65 (m, 5H), 7.81 (d, *J* = 7.1 Hz, 1H); ^{13}C NMR (75 MHz, $CDCl_3$) δ 109.3, 118.9 (estimated as 2C), 120.6, 123.0, 124.0, 126.8, 128.5, 129.4, 130.1, 130.5, 133.5, 133.9, 136.4, 141.8, 143.2; IR (KBr) 3124, 3052, 1610, 1601, 1516, 1508, 1484, 1305, 1292, 1235, 1206, 1057, 905, 830, 782, 764, 754, 662 cm^{-1}. HRMS (ESI) Calcd for $C_{20}H_{15}N_4$: $[M+H]^+$. 311.1291, found: *m*/*z* 311.1286. HRMS (ESI) Calcd for $C_{16}H_{12}N_4Na$: $[M+Na]^+$. 283.0954, found: *m*/*z* 283.0954.

Synthesis of 1,2-Bis(1*H*-benzo[*d*]imidazol-1-yl)benzene:[16] To a solution of 1-(2-bromophenyl)-1*H*-benzo[*d*]imidazole (1.914 g, 7.01 mmol), 1*H*-benzo[*d*]imidazole (0.998 g, 8.45 mmol), CuI (0.147 g, 0.770 mmol), L-proline (0.168 g, 1.46 mmol), and K_2CO_3 (1.937 g, 14.0 mmol) in DMSO (3.5 mL) was heated at 150 °C for 2 d. After cooling down to room temperature, to the reaction mixture was added EtOAc (10 mL) and brine (10 mL). After being extracted with EtOAc (10 mL × 4), the organic layer was washed with brine (10 mL). After drying with $MgSO_4$ and evaporation, the residue was subject to column chromatography on SiO_2 (hexane : EtOAc = 3 : 1 to 1 : 1) and preparative GPC (eluent: $CHCl_3$) to give 1,2-bis(1*H*-benzo[*d*]imidazol-1-yl)benzene (0.268 g, 0.862 mmol, 12%) as yellow solid. Recrystallization from hexane and $CHCl_3$ gave brown plate crystals: mp 205–207 °C; ^{1}H NMR (300 MHz, $CDCl_3$) δ 7.17-7.26 (m, 6H), 7.53 (s, 2H), 7.70 (s, 4H), 7.71 (d, *J* = 6.74 Hz, 2H); ^{13}C NMR (75 MHz, $CDCl_3$) δ 109.3, 120.7, 123.0, 124.0, 128.4, 130.0, 131.8, 133.7, 141.6, 143.2; IR (KBr) 3127, 3052, 1610, 1594, 1579, 1375, 1304, 1287, 1242, 1219, 1203, 1153, 1108, 1004, 984, 885, 868, 791, 766, 739, 631 cm^{-1}. HRMS (ESI) Calcd for $C_{20}H_{15}N_4$: $[M+H]^+$. 311.1291, found: *m*/*z* 311.1286.

Synthesis of 1-(2-Bromophenyl)-1*H*-indole:[7] To a solution of 1*H*-indole (2.370 g, 20.2 mmol), CuI (0.300 g, 1.58 mmol), K_3PO_4 (8.453 g, 39.8 mmol), 1,2-dibromobenzene (4.801 g, 20.4 mmol), and 1,2-ethylenediamine (0.268 g, 4.47 mmol) in toluene (3.5 mL) was heated at refluxing temperature for 2 d. After cooling down to room temperature, to the reaction mixture was filtered with a pad of Celite and Florizil®. After evaporation, the residue was subject to column chromatography on SiO_2 (first column; hexane : EtOAc = 2 : 1, and second column; hexane : $CHCl_3$ = 5 : 1) to give 1-(2-bromophenyl)-1*H*-

indole (2.237 g, 8.220 mmol, 41%) as colorless solid: ^{1}H NMR (300 MHz, DMSO-d_6) δ 6.69 (d, J = 3.0 Hz, 1H), 7.10 (m, 1H), 7.14-7.20 (m, 2H), 7.23 (d, J = 3.0 Hz, 1H), 7.33 (m, 1H), 7.41-7.44 (m, 2H), 7.68 (m, 1H), 7.77 (d, J = 7.8 Hz, 1H).[5]

Synthesis of 1-(2-(1*H*-Imidazol-1-yl)phenyl)-1*H*-indole:[16] To a solution of 1-(2-bromophenyl)-1*H*-indole (1.545 g, 5.68 mmol), 1*H*-imidazole (0.517 g, 7.59 mmol), Cu_2O (86.7 g, 0.606 mmol), and K_2CO_3 (1.643 g, 11.9 mmol) in DMSO (6 mL) was heated at 150 °C for 3 d. After cooling down to room temperature, to the reaction mixture was added EtOAc (10 mL) and brine (10 mL). After being extracted with EtOAc (30 mL × 4), the organic layer was washed with brine (10 mL). After drying with Na_2SO_4 and evaporation, the residue was subject to column chromatography on SiO_2 (hexane : EtOAc = 1 : 1 to only EtOAc) to give 1-(2-(1*H*-imidazol-1-yl)phenyl)-1*H*-indole (1.347 g, 5.19 mmol, 91%) as pale yellow oil. Recrystallization from hexane and $CHCl_3$ gave pale yellow cubic crystals: mp 104–105 °C; ^{1}H NMR (300 MHz, $CDCl_3$) δ 6.57 (d, J = 2.8 Hz, 1H), 6.57 (d, J = 1.0 Hz, 1H), 6.79 (d, J = 3.3 Hz, 1H), 6.88 (s, 1H), 7.12 (m, 3H), 7.28 (s, 1H), 7.47-7.63 (m, 5H); ^{13}C NMR (75 MHz, $CDCl_3$) δ 104.6, 109.4, 119.0, 120.6, 121.1, 122.7, 126.2, 127.3, 128.5, 128.8 (large intensity), 129.1, 129.8, 133.1, 133.8, 136.35, 136.41; IR (KBr) 3104, 3056, 1601, 1586, 1519, 1505, 1480, 1463, 1353, 1329, 1300, 1294, 1250, 1243, 1231, 1213, 1137, 1102, 1054, 964, 827, 776, 771, 765, 752, 729, 719, 662 cm^{-1}. HRMS (ESI) Calcd for $C_{17}H_{14}N_3$: $[M+H]^+$. 260.1182, found: m/z 260.1177.

Synthesis of Indolo[1,2-*a*]pyrrolo[2,1-*c*]quinoxaline (1-nB):[3] To a solution of 1-(2-(1*H*-pyrrol-1-yl)phenyl)-1*H*-indole (0.283 g, 1.10 mmol) in chlorobenzene (5 mL) was dropwise added a solution of I_2 (0.307 g, 1.21 mmol) in chlorobenzene (5 mL) in a period of 30 min. The mixture was stirred at room temperature. The dark precipitate was observed during the reaction proceeded. After being stirred for 24 h, to the reaction mixture was added saturated aqueous $Na_2S_2O_3$ solution (5 mL) and acetone (ca. 5 mL) to dissolve the precipitate. The combined mixture was extracted with $CHCl_3$ (5 mL × 3), and the organic layer was washed with brine (5 mL). After drying with $MgSO_4$ and evaporation, the residue was subject to column chromatography on SiO_2 (only hexane to hexane : EtOAc = 5 : 1) to give indolo[1,2-*a*]pyrrolo-[2,1-*c*]quinoxaline (**1-nB**) (0.243 g, 0.948 mmol, 87%) as brown solid. Recrystallization from hexane and $CHCl_3$ gave pale green needle crystals: mp 139–141 °C; ^{1}H NMR (300 MHz, $CDCl_3$) δ 6.63 (t, J = 3.4 Hz, 1H), 6.78 (d, J = 3.7 Hz, 1H), 6.88 (s, 1H), 7.29 (d, J = 7.4 Hz, 2H), 7.30-7.40 (m, 2H), 7.55 (s-like, 1H), 7.73 (t, J = 7.5 Hz, 2H), 8.21 (d, J = 8.1 Hz, 1H), 8.44 (d, J = 8.3 Hz, 1H); ^{13}C NMR (75 MHz, $CDCl_3$) δ 95.2, 104.6, 112.9, 113.4, 113.5, 115.4, 116.5, 120.8, 121.9, 122.0, 123.3, 123.5, 124.7, 125.6, 128.0, 129.7, 131.1, 133.5; IR (KBr) 3632, 3624, 3141, 1629, 1506, 1482, 1461, 1451, 1375, 1362, 1336, 1297, 1267, 1254, 1216, 1096, 774, 739, 721, 699 cm^{-1}. HRMS (ESI) Calcd for $C_{18}H_{13}N_2$: $[M+H]^+$. 257.1073, found: m/z 257.1072.

Synthesis of Imidazo[1,2-*a*]pyrrolo[2,1-*c*]quinoxaline (3-nn): To a solution of 1-(2-(1*H*-pyrrol-1-yl)phenyl)-1*H*-imidazole (0.216 g, 1.03 mmol) in THF (3 mL) was added a solution of *n*-BuLi (1.60 M in hexane, 0.69 mL, 1.10 mmol) at -40 °C. After being stirred for 40 min at that temperature, to the solution was added I_2 (0.292 g, 1.15 mmol). The reaction mixture was gradually warmed up to room temperature. After being stirred for 2 h, the reaction mixture was added saturated aqueous $Na_2S_2O_3$ solution (5 mL) and H_2O (5 mL). After being extracted with EtOAc (20 mL × 3), the organic layer was washed with brine (10 mL). After drying with $MgSO_4$ and evaporation, to the residue (0.353 g) was added $Pd(PPh_3)_4$ (0.121 g, 0.105 mmol), K_2CO_3 (0.363 g, 2.63 mmol), and DMF (5 mL). The combined mixture was heated at 100 °C for 3 d. After cooling down to room temperature, to the reaction mixture was added brine (5 mL), water (5 mL) and EtOAc (10 mL). The mixture was filtered with a pad of Celite and Florizil®. After being extracted with EtOAc (20 mL × 4), the organic layer was washed with brine (20 mL). After drying with $MgSO_4$ and evaporation, the residue was subjected to column chromatography on SiO_2 ($CHCl_3$: EtOAc = 3 : 1) and preparative GPC (eluent: $CHCl_3$) to give imidazo[1,2-*a*]pyrrolo[2,1-*c*]quinoxaline (**3-nn**) (0.106 g, 0.511 mmol, 50%) as pale brown solid. Recrystallization from acetone gave pale green needle crystals: mp 164–165 °C; ^{1}H NMR (300 MHz, $CDCl_3$) δ 6.65 (t, *J* = 3.2 Hz, 1H), 7.05 (d, *J* = 2.7 Hz, 1H), 7.23 (dt, *J* = 1.4 Hz and 7.4 Hz, 1H), 7.29 (dt, *J* = 1.5 and 7.4 Hz, 1H), 7.37 (s, 1H), 7.55 (d, *J* = 1.1 Hz, 1H), 7.57 (dd, *J* = 1.5 and 7.6 Hz, 1H), 7.60 (d, *J* = 1.2 Hz, 1H), 7.66 (dd, *J* = 1.5 and 7.6 Hz, 1H); ^{13}C NMR (75 MHz, $CDCl_3$) δ 104.7, 110.7, 113.0, 113.8, 115.3, 116.1, 121.8, 123.9, 124.7, 125.6, 125.7, 131.1, 138.2; IR (KBr) 3104, 1631, 1519, 1512, 1507, 1408, 1345, 1318, 1117, 741, 720, 706 cm^{-1}. HRMS (ESI) Calcd for $C_{13}H_{10}N_3$: $[M+H]^+$. 208.0869, found: *m*/*z* 208.0867.

Synthesis of Benzo[4,5]imidazo[1,2-*a*]pyrrolo[2,1-*c*]quinoxaline (3-nB): The titled compound was obtained in 34% yield (86.2 mg, 0.335 mmol) (two steps) from 1-(2-(1*H*-pyrrol-1-yl)phenyl)-1*H*-benzo[*d*]imidazole (0.254 g, 0.978 mmol) according to the similar procedure mentioned for **3-nn**: pale green needle crystals; mp 146–148 °C (hexane and $CHCl_3$); ^{1}H NMR (300 MHz, $CDCl_3$) δ 6.74 (t, *J* = 3.0 Hz, 1H), 7.33-7.44 (m, 5H), 7.69 (dd, *J* = 1.4 and 2.8 Hz, 1H), 7.78 (dd, *J* = 1.9 and 7.6 Hz, 1H), 7.89 (dd, *J* = 1.2 and 6.9 Hz, 1H), 8.08 (d, *J* = 7.5 Hz, 1H), 8.31 (dd, *J* = 1.8 and 7.8 Hz, 1H); ^{13}C NMR (75 MHz, $CDCl_3$) δ 108.5, 112.8, 113.7, 115.50, 115.52, 116.3, 120.0, 121.1, 122.9, 124.0, 125.0, 125.2, 125.4, 126.4, 131.1, 142.7, 144.9; IR (KBr) 3105, 1637, 1569, 1508, 1484, 1460, 1447, 1369, 1343, 1256, 1210, 741, 702 cm^{-1}. HRMS (ESI) Calcd for $C_{17}H_{12}N_3$: $[M+H]^+$. 258.1026, found: *m*/*z* 258.1021.

Synthesis of Benzo[4,5]imidazo[1,2-*a*]indolo[2,1-*c*]quinoxaline (3-BB): The titled compound was obtained in 53% yield (81.0 mg, 0.264 mmol) (two steps) from 1-(2-(1*H*-indol-1-yl)phenyl)-1*H*-benzo[*d*]imidazole (0.154 g, 0.499 mmol) according to the similar procedure mentioned for **3-nn**: light yellow solid; mp 199–200 °C (hexane and $CHCl_3$); ^{1}H NMR (300 MHz, DMSO-d_6, measured at 50 °C) δ 7.39 (t, *J* = 7.3 Hz, 1H), 7.45-7.58 (m, 5H), 7.61 (s, 1H), 7.87 (dd-like, *J* = 3.2 and 6.1 Hz, 1H), 7.92 (d, *J*

= 7.7 Hz, 1H), 8.46 (dd-like, *J* = 3.2 and 6.1 Hz, 1H), 8.52 (d, *J* = 8.6 Hz, 1H), 8.60 (d, *J* = 7.8 Hz, 1H), 8.68 (d, *J* = 8.1 Hz, 1H); ^{13}C NMR (75 MHz, DMSO-d_6, measured at 50 °C) δ 101.8, 113.8, 114.3, 116.67, 116.72, 119.7, 122.0, 122.5, 123.6, 124.0, 124.4, 124.6, 125.4, 125.8, 125.9, 127.0, 129.6, 130.8, 133.8, 141.9, 144.6; IR (KBr) 3106, 3047, 1637, 1572, 1519, 1501, 1484, 1468, 1448, 1381, 1344, 1326, 1302, 1292, 1263, 737 cm^{-1}. HRMS (ESI) Calcd for $C_{21}H_{14}N_3$: $[M+H]^+$. 308.1182, found: *m*/*z* 308.1175.

Synthesis of Benzo[4,5]imidazo[1,2-*a*]imidazo[2,1-*c*]quinoxaline (2-nB):[4] To a solution of 1-(2-(1*H*-imidazol-1-yl)phenyl)-1*H*-benzo[*d*]imidazole (0.581 g, 2.23 mmol) in THF (20 mL) was added a solution of *sec*-BuLi (1.03 M in cyclohexane/hexane, 5.2 mL, 5.36 mmol) at -78 °C. After being stirred for 1 h at that temperature, to the solution was added $Pd(PPh_3)_4$ (52.0 mg, 0.0450 mmol). The reaction mixture was gradually warmed up to 45 °C. After being stirred for 30 h, to the reaction mixture was added EtOAc (20 mL) and brine (20 mL). After being extracted with EtOAc (30 mL × 4), the organic layer was washed with brine (30 mL). After drying with $MgSO_4$ and evaporation, the residue was subject to column chromatography on SiO_2 ($CHCl_3$: MeOH = 10 : 1) to give benzo[4,5]imidazo[1,2-*a*]imidazo-[2,1-*c*]quinoxaline (**2-nB**) (0.556 g, 2.16 mmol, 96%) as pale brown oil. Recrystallization from hexane and $CHCl_3$ gave colorless solid: mp 243–245 °C; ^{1}H NMR (300 MHz, $CDCl_3$) δ 7.43-7.57 (m, 4H), 7.68 (s, 1H), 7.82 (d, *J* = 8.1 Hz, 1H), 7.90 (s, 1H), 8.03 (m, 1H), 8.16 (m, 1H), 8.42 (d, *J* = 8.3 Hz, 1H); ^{13}C NMR (75 MHz, $CDCl_3$) δ 113.1, 113.3, 116.5, 116.6, 121.6, 123.9, 124.1, 124.6, 125.4, 126.7, 126.8, 131.1, 133.7, 135.3, 139.7, 144.8; IR (KBr) 3110, 3052, 2924, 1637, 1568, 1503, 1486, 1465, 1447, 1401, 1362, 1317, 1305, 1284, 1259, 1240, 743, 724 cm^{-1}. HRMS (ESI) Calcd for $C_{16}H_{11}N_4$: $[M+H]^+$. 259.0978, found: *m*/*z* 259.0974.

Synthesis of Benzo[4,5]imidazo[1,2-*a*]benzo[4,5]imidazo[2,1-*c*]quinoxaline (2-BB): The titled compound was obtained in 56% yield (86.5 mg, 0.281 mmol) (two steps) from 1,2-bis(1*H*-benzo[*d*]imidazol-1-yl)benzene (0.155 g, 0.500 mmol) according to the similar procedure mentioned for **3-nn** by changing the reaction temperature (-60 °C) during the reaction with *sec*-BuLi: pale yellow needle crystals; mp 278 °C (dec.) (hexane and $CHCl_3$); ^{1}H NMR (300 MHz, DMSO-d_6, measured at 40 °C) δ 7.53-7.60 (m, 4H), 7.66 (dd-like, *J* = 3.1 and 6.0 Hz, 2H), 8.01 (m, 2H), 8.62 (m, 2H), 8.76 (dd-like, *J* = 3.5 and 6.1 Hz, 2H); ^{13}C NMR (75 MHz, DMSO-d_6, measured at 40 °C) δ 114.4, 116.9, 120.8, 124.7, 124.8, 125.7, 126.1, 131.0, 139.5, 144.3; IR (KBr) 2957, 1642, 1565, 1500, 1487, 1470, 1448, 1386, 1338, 1291, 740 cm^{-1}. HRMS (ESI) Calcd for $C_{20}H_{13}N_4$: $[M+H]^+$. 309.1135, found: *m*/*z* 309.1126.

Synthesis of Imidazo[1,2-*a*]indolo[2,1-*c*]quinoxaline (3-Bn): The titled compound was obtained in 46% yield (0.120 mg, 0.466 mmol) (two steps) from 1-(2-(1*H*-imidazol-1-yl)phenyl)-1*H*-indole (0.261 g, 1.01 mmol) according to the similar procedure mentioned for **3-nn**: pale blue needle crystals; mp 171–172 °C (acetone); ^{1}H NMR (300 MHz, $CDCl_3$) δ 7.18 (dt, *J* = 1.1 and 7.0 Hz, 1H), 7.27-7.37 (m, 4H), 7.42 (d, *J* = 1.4 Hz, 1H), 7.54 (d, *J* = 1.4 and 8.1 Hz, 1H), 7.60 (d, *J* = 1.4 Hz, 1H), 7.77 (dd, *J* = 1.6 and 7.2 Hz,

1H), 8.10 (d, J = 8.4 Hz, 1H), 8.29 (dd, J = 1.1 and 8.4 Hz, 1H); ^{13}C NMR (75 MHz, $CDCl_3$) δ 88.8, 111.7, 113.5, 116.1, 116.3, 122.0, 122.3, 123.4, 123.5, 123.7, 126.0, 126.8, 128.1, 130.2, 132.0, 133.7, 137.8; IR (KBr) 3085, 3047, 1633, 1522, 1507, 1489, 1469, 1450, 1409, 1356, 1239, 1104, 927, 781, 739, 724 cm^{-1}. HRMS (ESI) Calcd for $C_{17}H_{12}N_3$: $[M+H]^+$. 258.1026, found: m/z 258.1020.

X-Ray Crystallography: X-Ray diffraction data for the crystals were measured on a Bruker APEXII CCD diffractometer with graphite-monochromated Mo Kα (λ = 0.71073 Å) radiation. Data collections were carried out at 173 K. All structures were solved by a direct method SHELXS-97,[17] and the non-hydrogen atoms were refined anisotropically against F^2, with full-matrix least-squares methods SHELEXL-97[18] in a computer program package from Bruker AXS. All hydrogen atoms were positioned geometrically and refined as riding. Crystal data for **1-nn**: $C_{14}H_{10}N_2$, monoclinic, $P2_1/c$, Z = 8, a = 5.4161(6) Å, b = 16.2831(19) Å, c = 23.026(3) Å, β = 92.6400(15)°, V = 2028.5(4) Å^3, R_1 = 0.0637, wR_2 = 0.1989, T = 173 K. Crystal data for **3-nn**: $C_{13}H_9N_3$, monoclinic, $P2_1/n$, Z = 4, a = 6.9518(9) Å, b = 10.4546(14) Å, c = 13.6988(17) Å, β = 95.4018(19)°, V = 991.2(2) Å^3, R_1 = 0.0463, wR_2 = 0.1228, T = 173 K. Deposition number CCDC-1038082 (**1-nn**) and CCDC-1038083 (**3-nn**). Copies of the data can be obtained free of charge via www.ccdc.cam.ac.uk/conts/retrieving.html (or from the Cambridge Crystallographic Data Centre, 12, Union Road, Cambridge, CB2 1EZ, UK; Fax.: +44 1223 336033; e-mail: deposit@ccdc.cam.ac.uk).

ACKNOWLEDGEMENTS

This work was supported by JSPS KAKENHI Grant No. 24550146.

REFERENCES AND NOTES

1. For recent examples: (a) K. Matsuo, S. Saito, and S. Yamaguchi, *J. Am. Chem. Soc.*, 2014, **136**, 12580; (b) L. Wang, Y. Shen, M. Yang, X. Zhang, W. Xu, Q. Zhu, J. Wu, Y. Tian, and H. Zhou, *Chem. Commun.*, 2014, **50**, 8723; (c) S. Y. Lee, T. Yasuda, Y. S. Yang, Q. Zhang, and C. Adachi, *Angew. Chem. Int. Ed.*, 2014, **53**, 6402; (d) J. Zhang and W. Guo, *Chem. Commun.*, 2014, **50**, 4214; (e) K. Tateno, R. Ogawa, R. Sakamoto, M. Tsuchiya, T. Otani, and T. Saito, *Org. Lett.*, 2014, **16**, 3212; (f) C. Saravanan, S. Easwaramoorthi, C.-Y. Hsiow, K. Wang, M. Hayashi, and L. Wang, *Org. Lett.*, 2014, **16**, 354; (g) B. Neute, J. F. Araneda, W. E. Piers, and M. Parvez, *Angew. Chem. Int. Ed.*, 2013, **52**, 9966; (h) X. Wang, F. Zhang, J. Liu, R. Tang, Y. Fu, D. Wu, Q. Xu, X. Zhuang, G. He, and X. Feng, *Org. Lett.*, 2013, **15**, 5714; (i) C. Yuan, S. Saito, C. Camacho, S. Irle, I. Hisaki, and S. Yamaguchi, *J. Am. Chen. Soc.*, 2013, **135**, 8842; (j) M. R. Aronoff, B. VanVeller, and R. T. Raines, *Org. Lett.*, 2013, **15**, 5382; (k) L. Yang, J. Ye, Y. Gao, D. Deng, W. Gong, Y. Lin, and G. Ning,

Tetrahedron Lett., 2013, **54**, 2967; (l) L. Zöphel, V. Enkelmann, and K. Müllen, *Org. Lett.*, 2013, **15**, 804; (m) S. Yang, J. You, J. Lan, and G. Gao, *J. Am. Chem. Soc.*, 2012, **134**, 11868; (n) M. Grybowski, M. E. Glodkowska-Mrowka, T. Stoklosa, and D. T. Gryko, *Org. Lett.*, 2012, **14**, 2670; (o) J. Chen, W. Lin, J. Ma, H. Xu, J. Wu, X. Tang, Z. Fan, and P. Wang, *J. Org. Chem.*, 2012, **77**, 3475; (p) J. Massue, D. Frath, G. Ulrich, P. Retailleau, and R. Ziessel, *Org. Lett.*, 2012, **14**, 230.

2. (a) D. S. Pisoni, L. Todeschini, A. C. A. Borges, C. L. Petzhold, F. S. Rodembusch, and L. F. Campo, *J. Org. Chem.*, 2014, **79**, 5511; (b) S. Cho, Y. Lee, H. S. Han, H. K. Lee, and S. Jeon, *J. Phys. Chem. A*, 2014, **118**, 4995; (c) Y. Deng, Y.-Y. Cheng, H. Liu, J. Mack, H. Lu, and L.-G. Zhu, *Tetrahedron Lett.*, 2014, **55**, 3792; (d) L. Li, P. Wang, Y. Zhang, Y. Wu, Z. Chen, and C. He, *J. Mol. Struct.*, 2013, **1051**, 23; (e) M.-S. Yuan, Q. Wang, W.-J. Wang, T.-B. Li, L. Wang, W. Deng, Z.-T. Du, and J.-R. Wang, *Dyes Pigments*, 2012, **95**, 236; (f) I. Garcia-Moreno, W. Lu, A. Costeral, J. Banuelos, A. Lopez, and X. Y. Inigo, *ChemPhysChem*, 2012, **13**, 3923; (g) Y. Gong, X. Guo, S. Wang, H. Su, A. Xia, Q. He, and F. Bai, *J. Phys. Chem. A*, 2007, **111**, 5806; (h) S. Amthor, C. Lambert, S. Dümmler, I. Fischer, and J. Schelter, *J. Phys. Chem. A*, 2006, **110**, 5204.
3. S. Matsumoto, S. Qu, T. Kobayashi, M. Kanehiro, M. Akazome, and K. Ogura, *Heterocycles*, 2010, **80**, 645.
4. S. Matsumoto, E. Batmunkh, M. Akazome, Y. Takata, and M. Tamano, *Org. Biomol. Chem.*, 2011, **9**, 5941.
5. D. G. Hulcoop and M. Lautens, *Org. Lett.*, 2007, **9**, 1761.
6. K. Hirano, A. T. Biju, and F. Glorius, *J. Org. Chem.*, 2009, **74**, 9570.
7. J. C. Antilla, A. Klapars, and S. L. Buchwald, *J. Am. Chem. Soc.*, 2002, **124**, 11684.
8. Gaussian 09, Revision A.02, M. J. Frisch, G. W. Trucks, H. B. Schlegel, G. E. Scuseria, M. A. Robb, J. R. Cheeseman, G. Scalmani, V. Barone, B. Mennucci, G. A. Petersson, H. Nakatsuji, M. Caricato, X. Li, H. P. Hratchian, A. F. Izmaylov, J. Bloino, G. Zheng, J. L. Sonnenberg, M. Hada, M. Ehara, K. Toyota, R. Fukuda, J. Hasegawa, M. Ishida, T. Nakajima, Y. Honda, O. Kitao, H. Nakai, T. Vreven, J. A. Montgomery, Jr., J. E. Peralta, F. Ogliaro, M. Bearpark, J. J. Heyd, E. Brothers, K. N. Kudin, V. N. Staroverov, R. Kobayashi, J. Normand, K. Raghavachari, A. Rendell, J. C. Burant, S. S. Iyengar, J. Tomasi, M. Cossi, N. Rega, J. M. Millam, M. Klene, J. E. Knox, J. B. Cross, V. Bakken, C. Adamo, J. Jaramillo, R. Gomperts, R. E. Stratmann, O. Yazyev, A. J. Austin, R. Cammi, C. Pomelli, J. W. Ochterski, R. L. Martin, K. Morokuma, V. G. Zakrzewski, G. A. Voth, P. Salvador, J. J. Dannenberg, S. Dapprich, A. D. Daniels, O. Farkas, J. B. Foresman, J. V. Ortiz, J. Cioslowski, and D. J. Fox, Gaussian, Inc., Wallingford CT, 2009.
9. An orbital similar to the HOMO of **2-BB** in TDDFT calculation is present as HOMO-1 in DFT calculation, which lies on a little lower energy level than the HOMO in DFT calculation (Figure S2).

Thus, the transition from degenerated HOMO and HOMO-1 to LUMO is plausible by the photoexcitation. However, there is relatively large energy gap between HOMO and HOMO-1 in TDDFT calculation.

10. (a) S. Kumar, P. Singh, R. Srivastava, R. R. Koner, A. Pramanik, J. Mathew, S. Sinha, M. Rawat, R. S. Anand, and S. Ghosh, *J. Mater. Chem. C*, 2014, **2**, 6637; (b) K. Shirai, M. Matsuoka, and K. Fukunishi, *Dyes Pigments*, 1999, **42**, 95.
11. (a) P. Wang, C. J. Collison, and L. J. Rothlberg, *J. Photochem. Photobiol. A*, 2001, **144**, 63; (b) R. Jakubiak, C. J. Collison, W. C. Wan, and L. J. Rothberg, *J. Phys. Chem. A*, 1999, **103**, 2394; (c) L. J. Rothberg, M. Yan, F. Papadimitrakopoulos, M. E. Galvin, E. W. Kwock, and T. M. Miller, *Synth. Met.*, 1996, **80**, 41.
12. A. Bondi, *J. Phys. Chem.*, 1964, **68**, 441.
13. (a) M. Cigáň, J. Donovalová, V. Szöcs, J. Gašpar, K. Jakusová, and A. Gáplovský, *J. Phys. Chem. A*, 2013, **117**, 4870; (b) H. Yao and K. Ashiba, *RSC Adv.*, 2011, **1**, 834; (c) V. Lau and B. Heyne, *Chem. Commun.*, 2010, **46**, 3595.
14. (a) S. Chakraborty, P. Debnath, D. Dey, D. Bhattacharjee, and S. A. Hussain, *J. Photochem. Photobiol. A*, 2014, **293**, 57; (b) F. Würthner, Z. Chen, V. Dehm, and V. Stepanenko, *Chem. Commun.*, 2006, 1188; (c) B. Jancy and S. K. Asha, *Chem. Mater.*, 2008, **20**, 169; (d) L. Wang, Y. Shen, M. Yang, X. Zhang, W. Xu, Q. Zhu, J. Wu, Y. Tian, and H. Zhou, *Chem. Commun.*, 2014, **50**, 8723; (e) U. Rösch, S. Yao, R. Wortmann, and F. Würthner, *Angew. Chem. Int. Ed.*, 2006, **45**, 7026.
15. Q. Cai, Z. Li, J. Wei, L. Fu, C. Ha, D. Pei, and K. Ding, *Org. Lett.*, 2010, **12**, 1500.
16. Y.-H. So, *Macromolecules*, 1992, **25**, 516.
17. G. M. Sheldrick, *SHELX97. Acta Crystallogr., Sect. A*, 2008, **64**, 112.
18. G. M. Sheldrick, *SHELXTL*, Version 5.10, Bruker AXS, Madison, Wisconsin, USA, 1997.